

# Global analysis of isospin dependent microscopic nucleon-nucleus optical potential in Dirac Bruckner Hartree-Fock approach

Ruirui Xu,<sup>\*</sup> Zhongyu Ma,<sup>†</sup> Yue Zhang, and Yuan Tian  
*China Institute of Atomic Energy, P.O. Box 275(41), Beijing 102413, China*

E. N. E. van Dalen and H. Mütter<sup>‡</sup>  
*Institut für Theoretische Physik, Universität Tübingen,  
 Auf der Morgenstelle 14, D-72076 Tübingen, Germany*  
 (Dated: May 26, 2016)

**Background:** For the study of exotic nuclei it is important to have an optical model potential, which is reliable not only for stable nuclei but can also be extrapolated to nuclear systems with exotic numbers of protons and neutrons. An effective way to obtain such a potential is to develop a microscopic optical potential (MOP) based on a fundamental theory with a minimal number of free parameters, which are adjusted to describe stable nuclei all over the nuclide chart.

**Purpose:** The choice adopted in the present work is to develop the MOP within a relativistic scheme which provides a natural and consistent relation between the spin-orbit part and the central part of the potential. The Dirac-Brueckner-Hartree-Fock (DBHF) approach provides such a microscopic relativistic scheme, which is based on a realistic nucleon-nucleon interaction and reproduce the saturation properties of symmetric nuclear matter without any adjustable parameter. Its solution using the projection technique within the subtracted T-matrix (STM) representation provides a reliable extension to asymmetric nuclear matter, which is important to describe the features of the isospin asymmetric nuclei. Therefore, the present work aims to perform a global analysis of the isospin-dependent nucleon-nucleus MOP based on the DBHF calculation in symmetric and asymmetric nuclear matter.

**Methods:** The DBHF is used to evaluate the relativistic structure of the nucleon self-energies in nuclear matter at various densities and asymmetries. The Schrödinger equivalent potentials of finite nuclei are derived from these Dirac components by a local density approximation (LDA). The density distributions of finite nuclei are taken from the Hartree-Fock-Bogoliubov (HFB) approach with Gogny D1S force. An improved LDA approach (ILDA) is employed to get a better prediction of the scattering observables. A  $\chi^2$  assessment system based on the global simulated annealing algorithm (GSA) is developed to optimize the very few free components in this study.

**Results:** The nucleon-nucleus scattering calculations are carried out for a broad spectrum  $n$  and  $p$  scattering experiments below 200 MeV with targets ranging from  $^{12}\text{C}$  to  $^{208}\text{Pb}$ . The scattering observables including the neutron total cross section, proton reaction cross section, elastic scattering angular distribution, analyzing power and spin rotation are evaluated and compared with the experimental data, as well as with results derived from the widely used phenomenological Koning-Delaroche (KD) global potential.

**Conclusions:** Results with the present relativistic MOP satisfactorily reproduce the  $n, p + A$  scattering observables over a broad mass range and a large energy region only with the free range factor  $t$  in ILDA and minor adjustment to the scalar and vector potentials around the low density region, and the relevant potentials are physically well-behaved. The overall agreement indicates that the present MOP may have predictive power for unstable nuclei, as well as the nuclei beyond the line of  $\beta$  stability.

PACS numbers: 24.10.Ht; 24.10.Cn; 24.10.Jv; 21.65.Cd

## I. INTRODUCTION

The nuclear reaction of unstable nuclei is of high interest in the contemporary fundamental physics as well as applied nuclear physics. The corresponding information from experimental data is always too sparse or totally lacking. Therefore, during the past few decades, consid-

erable effort has been made to explore the nuclear reaction based on a fundamental microscopic nuclear theory so as to obtain more reliable prediction.

The optical model is the crucial component in the nuclear reaction study, mainly because it determines the cross section for nuclear scattering and compound nuclear formation in the initial stage of a reaction and supplies the transmission coefficients for branching into the various final states [1]. Many observables such as the elastic scattering angular distribution, analyzing power, spin rotation function and so on can be derived through the optical model. Therefore, the most important criteria to assess a microscopic optical potential (MOP) is that

<sup>\*</sup>xuruirui@ciae.ac.cn

<sup>†</sup>mazy12@ciae.ac.cn

<sup>‡</sup>herbert.muether@uni-tuebingen.de

it can reproduce the existing experimental data of these observables as accurate as possible, and make a reliable prediction without experimental guidance. Furthermore, the MOP is more appealing when it is established on better theoretical grounds with a small number of free parameters.

In the direct evaluation for MOP of finite nuclei an attempt is made to evaluate the scattering and absorption processes using a many-body theory for the target nuclei which goes beyond mean field theory and incorporates e.g. the effects of particle-vibration couplings. These studies typically employ an effective nucleon-nucleon ( $NN$ ) interaction (e.g. Skyrme interaction or Gogny interaction). Recently, several investigations for finite nuclei have been reported [2, 3], however, it seems still infeasible to derive the MOP for all nuclei, which are of interest e.g. in the field of applications of nuclear physics. In addition the specification of a sound nuclear structure for targets, especially for exotic nuclei remains to be progressed. Using phenomenological  $NN$  interactions such calculations are designed to derive the nuclear structure and the MOP from the same interaction model. A drawback of this scheme is phenomenological and fitted to describe these data.

On the other hand, various attempts have been made to derive the MOP from a realistic model of the  $NN$  interaction, which means an interaction designed and fitted to describe the  $NN$  scattering data. Such studies often use the system of nuclear matter to determine the effects of correlations and evaluate the medium dependence of the resulting effective interaction for nuclear matter. The nuclear matter results are then used in various kinds of local density approximation (LDA) to be applicable for finite nuclei. The review article of Ray et al. discusses various approximation schemes along this line [4].

Pioneering work along this line has been presented by Mahaux and coworkers [6] who evaluated the nucleon self-energy in nuclear matter as a function of density and energy in a Brueckner Hartree Fock (BHF) approximation and identified the resulting complex single-particle potential with the MOP for finite nuclei using LDA adopting nucleon density distributions from the empirical formula or microscopic nuclear structure calculations. One drawback of this scheme is that typically one has to use an interaction model for the evaluation of the density profile of the nuclei which is different from the realistic interaction used to calculate the self-energy in nuclear matter as BHF calculations fail to reproduce the empirical saturation properties for nuclear matter and finite nuclei. In a simplified way, some MOPs have been developed by adopting the effective  $NN$  interactions (e.g. Skyrme force) in the Hartree-Fock approach in nuclear matter and LDA for finite nuclei [5].

Another handicap of this approach is the fact that this approach only provides the central part of the MOP, the spin-orbit potential has to be adjusted independently from the central potential in such a non-relativistic approach. Nevertheless this scheme has been applied with

quite some success by Jeukenne, Lejeune and Mahaux already in the 1970s [6] and is still rather popular today.

Also the so-called  $g$ -folding method developed by Amos et al. [7] is based on a realistic  $NN$  interaction and uses a local density approximation to account for the medium dependence of the effective interaction. In this case, however, it is the  $NN$  interaction, which is evaluated by solving the Bethe-Goldstone equation in nuclear matter and then employed in a folding calculation to evaluate the MOP for finite nuclei. The  $g$ -folding approach has very successfully been applied to reproduce differential cross sections and spin observables in an energy range from 30 MeV to 300 MeV in several nuclei without any adjustment of parameters [7–13].

The Mahaux scheme as well as the “ $g$ ”-folding method are based on a non-relativistic approach and the energy-dependence of the MOP originates from the energy-dependence of the effective interaction  $g$  calculated for nuclear matter in the BHF approximation.

An alternative approach is based on the Dirac phenomenology as it has been introduced by Walecka and coworkers [14]. Within this Dirac phenomenology the nucleon self-energy contains a large and attractive component, which transforms like a scalar under a Lorentz transformation compensated to a large extent by a repulsive Lorentz vector component. If one reduces the corresponding Dirac equation for the nucleon in the nuclear matter medium to a non-relativistic Schrödinger equation, one obtains a Schrödinger equivalent potential with a central potential which is energy dependent and a strong spin-orbit term.

An application of this Dirac phenomenology to describe the optical model potential has been presented by Cooper et al. [15]. They developed a phenomenological parametrization of the real and imaginary parts of the scalar and vector potentials. Fitting the corresponding parameters, which depend on energy and mass number of the target nucleus, they obtain a very good global fit of the optical model potential.

A comparison of the rather successful but very different approaches to a global optical potential, the  $g$ -folding method and Dirac phenomenology, has been made by Deb et al. [10]. They evaluated differential cross sections and spin observables for nucleon nucleus scattering on five different targets ranging from  $^{12}\text{C}$  to  $^{208}\text{Pb}$  at energies of 65 and 200 MeV using both approaches and conclude that the results are of similar quality.

It is one aim of the Dirac Brueckner Hartree Fock (DBHF) approach, to combine the features of a realistic  $NN$  interaction and its dependence on the medium, as they are contained in the Mahaux approach and the “ $g$ ”-folding model with those of the Dirac phenomenology [16]. This approach is founded on a realistic  $NN$  interaction and the treatment of nuclear correlations and the medium dependence of the effective  $NN$  interaction is done in straight analogy to the Mahaux approach and the  $g$ -folding method. The DBHF approach, however, keeps track of the relativistic structure of the nucleon

self-energy and therefore one can determine the real and imaginary part of the scalar and vector component of the nucleon self-energy in nuclear matter as a function of momentum, density and energy. These components are then used to evaluate the corresponding MOP using LDA for these components of the self-energy in straight analogy to the Mahaux scheme.

In this way, the spin-orbit potential arises naturally from the coherent sum of the contribution from the scalar and vector potentials in this relativistic scheme, and the saturation properties of symmetric nuclear matter are reproduced in the relativistic Dirac Brueckner-Hartree-Fock (DBHF) approach, while three-nucleon forces have to be introduced to obtain a corresponding result within the non-relativistic BHF approximation [17–19]. Therefore it seems rather attractive to determine a microscopic optical model based on the DBHF approach as finally one may be able to describe the ground-state properties of nuclei and the MOP within the same theoretical framework.

For a long period it has been a challenge in theoretical nuclear physics to solve the Brueckner-Hartree-Fock in the relativistic way, especially for isospin asymmetric nuclear matter. In recent years substantial progress has been obtained using a so-called subtracted T-matrix (STM) representation in the projection technique to solve DBHF strictly in the symmetric and asymmetric nuclear matter [20].

In a preliminary study we have explored the isospin dependent relativistic microscopic optical potential adopting the self-energies from this DBHF calculation in [16]. This MOP has been verified by satisfactorily reproducing the neutron and proton scattering data from  $^{27}\text{Al}$ . In this work, a systematic investigation for this MOP is performed in a large range of nuclei. The microscopic radial nucleon density of finite nuclei based on the Hartree-Fock-Bogoliubov (HFB) calculation are adopted in this calculation instead of the previous empirical values. Meanwhile, a  $\chi^2$  assessment system based on the global simulated annealing algorithm (GSA) is specially designed to optimize the free factors and give an overall estimation on the performance of this MOP.

The paper is composed as follows. In Section II, the general formalism of DBHF is briefly introduced. The isospin dependent relativistic MOP of finite nuclei are built in Section III through combining the self-energies and the microscopic radial nucleon density by the improved local density approximation (ILDA) [6]. The global analysis of nuclear scattering is carried out in Section IV for neutron and proton scattering and induced reactions on  $^{12}\text{C}$  -  $^{208}\text{Pb}$  and the calculated results are compared with the calculated results with the widely-used phenomenological Koning-Delaroche (KD) global optical potential [21] and the experimental data of various scattering quantities. Finally, the overall discussion is summarized in Section V.

## II. SELF-ENERGY IN NUCLEAR MATTER

Realistic  $NN$  interactions contain strong short-range and tensor components. Therefore it is necessary to account for the corresponding correlations between the interacting nucleons. In the relativistic Brueckner-Hartree-Fock approach this is achieved by considering the equation for two interacting nucleons in nuclear matter. This leads to the ladder approximation of the relativistic Bethe-Salpeter (BS) equation [20, 22],

$$T = V + i \int V Q G G T, \quad (1)$$

where  $T$  is the nucleon-nucleon interaction matrix in the nuclear medium and  $V$  is the bare  $NN$  interaction, respectively. The Pauli exclusion principle is included by the  $Q$  operator and the in-medium nucleon propagation of the nucleons is described by the Green's function  $G$ , which fulfills the Dyson equation,

$$G = G_0 + G_0 \Sigma G. \quad (2)$$

$G_0$  denotes the free nucleon propagator, and the self-energy term  $\Sigma$  is defined in first order of the effective interaction  $T$  through the following standard Hartree-Fock equation

$$\Sigma = -i \int_F (Tr[GT] - GT). \quad (3)$$

Note the self-energy contains the direct and exchange terms at the same time, and that the momentum integration considers all nucleon states within the Fermi sea represented by  $F$  in Eq. 3. Because Eqs. 1-3 are strongly coupled, they have to be solved iteratively until convergence is reached.

Generally, the Lorentz structure of the relativistic self-energy  $\Sigma$  can be expressed as [23],

$$\Sigma^m(k, k_F, \beta) = \Sigma_s^m(k, k_F, \beta) - \gamma_0 \Sigma_0^m(k, k_F, \beta) + \gamma \cdot \mathbf{k} \Sigma_v^m(k, k_F, \beta). \quad (4)$$

In this equation,  $\Sigma_s$  is the scalar part of self-energy,  $\Sigma_0$  and  $\Sigma_v$  denote the time-like and space-like terms of the vector part, respectively. The superscript  $m$  is used to sign the proton and neutron since they should be distinguished in isospin asymmetric nuclear matter. Note that these components of the self-energy are functions of the nucleon momentum ( $k$ ), density or Fermi momentum ( $k_F$ ), and asymmetry parameter  $\beta = (\rho_n - \rho_p)/\rho$ , where  $\rho_n$ ,  $\rho_p$  and  $\rho$  indicate the neutron, proton and total densities in nuclear matter, respectively.

Details of such DBHF calculations and the method to extract these Dirac components using the subtracted T-matrix (STM) representation are described in [20, 24, 25]. The self-energies used in the present study are determined using the Bonn-B potential [26] for the bare  $NN$  interaction and solving the DBHF equations for isospin asymmetric nuclear matter with various densities and isospin asymmetries.

### III. RELATIVISTIC MICROSCOPIC OPTICAL POTENTIAL IN FINITE NUCLEI

In the relativistic scheme, the wave function of an incident particle described in terms of a Dirac spinor  $\Psi$  is obtained by the solution of the corresponding Dirac equation,

$$[\vec{\alpha} \cdot \vec{p} + \gamma_0(M + U_s^m) + U_0^m] \Psi^m = \varepsilon \Psi^m, \quad (5)$$

where  $U_s^m$  and  $U_0^m$  are the scalar and vector components of the scattering potential

$$U_s^m = \frac{\Sigma_s^m - \Sigma_v^m M}{1 + \Sigma_v^m}, \quad U_0^m = \frac{-\Sigma_0^m + \varepsilon \Sigma_v^m}{1 + \Sigma_v^m}, \quad (6)$$

and  $\varepsilon = E + M$  is the single particle energy,  $E$  is the kinetic energy of the nucleon in the free space and  $M$  indicates the mass of the nucleon.

In order to calculate the scattering observables of finite nuclei this Dirac equation is typically reduced to a Schrödinger type equation by eliminating the lower components of the Dirac spinor in a standard way. The equation for the upper components of the wave function is transformed into:

$$\left[ -\frac{\nabla^2}{2\varepsilon} + V_{cent}^m + V_{s.o.}^m(r) \vec{\sigma} \cdot \vec{\mathbf{L}} + V_{Darwin}^m(r) \right] \varphi(\mathbf{r}) = \frac{\varepsilon^2 - M^2}{2\varepsilon} \varphi(\mathbf{r}), \quad (7)$$

where  $V_{cent}^m$ ,  $V_{s.o.}^m$ , and  $V_{Darwin}^m$  represent the Schrödinger equivalent central, spin-orbit and Darwin potentials, respectively. The potentials in Eq. 8 are obtained from the scalar  $U_s$  and vector  $U_0$  potentials as

$$V_{cent}^m = \frac{M}{\varepsilon} U_s^m + U_0^m + \frac{1}{2\varepsilon} [U_s^{m2} - (U_0^m + V_c)^2],$$

$$V_{s.o.}^m = -\frac{1}{2\varepsilon r D^m(r)} \frac{dD^m(r)}{dr}, \quad (8)$$

$$V_{Darwin}^m = \frac{3}{8\varepsilon D^m(r)} \left[ \frac{dD^m(r)}{dr} \right]^2 - \frac{1}{2\varepsilon r D^m(r)} \frac{dD^m}{dr} - \frac{1}{4\varepsilon D^m(r)} \frac{d^2 D^m(r)}{d^2 r},$$

where  $V_c$  is the Coulomb potential for a charged particle and  $D$  denotes a quantity defined as

$$D^m(r) = M + \varepsilon + U_s^m(r) - U_0^m(r) - V_c. \quad (9)$$

The radial potentials in finite nuclei, namely  $V_{cent}^m$ ,  $V_{s.o.}^m$ , and  $V_{Darwin}^m$  in Eqs. (8)-(9), can be associated with the scalar  $U_s$  and vector  $U_0$  in nuclear matter through the local density approximation (LDA) using the local nucleon density  $\rho(r)$  for the nucleus considered. In this work, a finite range correction in Gaussian form is

adopted in LDA to further remedy the potentials to obtain the better prediction of the scattering experimental data, that is the so-called improved local density approximation (ILDA),

$$U_{ILDA}(r, E) = (t\sqrt{\pi})^{-3} \times \int U_{LDA}(r', E) \exp(-|\vec{r} - \vec{r}'|^2/t^2) d^3 r', \quad (10)$$

where  $t$  is an effective range parameter of the potential  $U_{LDA}$  in normal LDA approach at radius  $r'$ . It is included to account for a finite-range correction of the nucleon-nucleon interaction, which is not incorporated in the DBHF calculation. They modify the radial distribution of  $V_{cent}$  while keep its volume integral constant. The potential  $U_{LDA}$  is related to the  $U_s$  and  $U_0$  in nuclear matter by

$$U_{LDA}(r, E) = U_{NM}(k, E, \rho(r), \beta(r)), \quad (11)$$

and  $U_{NM}$  represent the corresponding potential in nuclear matter using the isospin asymmetry  $\beta$  of the target nucleus and the momentum  $k$  and energy  $E$  of the incoming nucleon. In our present studies we adopt the radial nucleon density,  $\rho(r)$ , from the Hartree-Fock-Bogoliubov (HFB) approach with Gogny D1S force [27], instead of the empirical values by the Negele's formula [28], which has been employed for our pilot study [16].

In Fig. 1, we compare the radial density and asymmetry distributions for  $^{208}\text{Pb}$  as derived from HFB approach and the empirical formula. The radial densities obtained in the HFB approach show oscillations in the interior of the nucleus, which reflect the structure of the single-particle wave functions. Note, however, that the oscillations are smoothed out to a large extent in the ILDA potentials by the finite range correction of Eq. 10. Also note the enhancement of the neutron density in the surface of the nucleus in the microscopic calculation. This neutron skin leads to large isospin asymmetries as presented in the left panel of Fig. 1.

In addition, as for this microscopic optical potential, the applicability of the theory should be indicated that the formalism does not include the coupling to giant resonances (10 MeV to 30 MeV) and the compound nucleus formation ( $< 10$  MeV), which has been discussed before and stressed in e.g. [7]. At the low energies, we include the compound nuclear contribution to the elastic differential cross sections by the Hauser-Feshbach statistic theory through the optical model code APMN [29], which employs the Hauser-Feshbach model to determine the contributions from the compound nuclear elastic scattering by concerning six competing single-particle emission reactions, including neutron, proton, deuteron, tritium,  $\alpha$ , and  $^3\text{He}$ . The formation of giant resonances will further discussed in other future work.

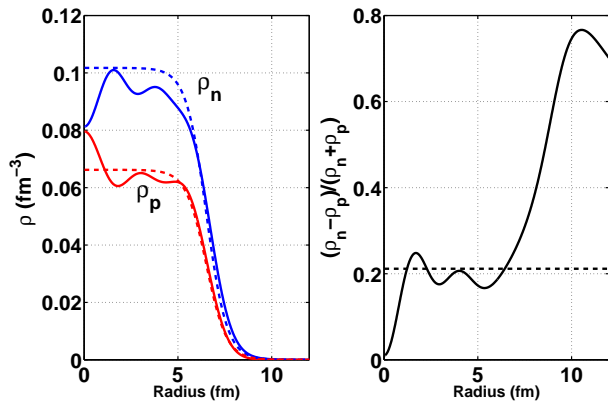


FIG. 1: (color online) The proton and neutron radial densities for  $^{208}\text{Pb}$ . The solid and dashed lines indicate the calculated results from HFB and the Negele's empirical formula, respectively.

#### IV. GLOBAL ANALYSIS OF NUCLEON-NUCLEI RMOP

##### A. Dirac potentials in the density region relevant for finite nuclei

It is the aim of this work to generate an optical potential, which has a microscopic basis and reproduces bulk features of nucleon-nucleus scattering for nuclei across the whole nuclide chart. The microscopic basis of these calculations originates from the real and imaginary parts of the Dirac components,  $U_s^m$  and  $U_0^m$ , of the nucleon self-energies calculated in the DBHF approach for symmetric and asymmetric nuclear matter. Such DBHF calculations, however, yield reliable results only for densities  $\rho > 0.08 \text{ fm}^{-3}$ . The procedure to derive self-consistent DBHF results does typically not converge at lower densities. This reflects the situation that homogeneous nuclear matter is unstable at such low densities with respect to the formation of an inhomogeneous density profile containing nuclear clusters. In particular the solution of the  $T$ -matrix of Eq. 1 yields bound states in the deuteron channel.

For the derivation of the optical model potential for finite nuclei, however, we also need results at densities  $\rho < 0.08 \text{ fm}^{-3}$ . Therefore we have to extrapolate the results to these low densities with the natural constraint that the Dirac potentials  $U_s^m$  and  $U_0^m$  vanish at  $\rho = 0$ . A linear interpolation of these Dirac potentials between  $\rho = 0.08 \text{ fm}^{-3}$  and  $\rho = 0$  might be too simple. Therefore we have introduced auxiliary mesh-points at  $\rho = 0.04 \text{ fm}^{-3}$  for the real parts and at  $\rho = 0.04$  and  $0.06 \text{ fm}^{-3}$  for the imaginary parts. The values of the linear interpolation at these auxiliary mesh-points is then enhanced by a factor  $f_1$  for the real part and a factor  $f_2$  for the imaginary part. Typical value for these enhancement factors ( $f_1, f_2$ ) are (0.86, 1.14) (see description of fitting procedure below).

Since the evaluation of the spin-orbit and Darwin potential (see Eq. 8) requires the calculation of derivatives of the Dirac potentials with respect to their density dependence, it is favorable to determine a simple interpolation scheme, which is valid for all densities entering into the calculation. Therefore we have chosen to represent the density-dependence of the Dirac potentials in terms of a polynomial fit with a polynomial of degree 5 for the real part and a polynomial of degree 7 for the imaginary part. The coefficients of these polynomials are determined to fit the results at all calculated densities, including the auxiliary mesh points mentioned above.

As an example we present in Fig. 2 values for the real and imaginary parts of the Dirac potentials  $U_s^m$  and  $U_0^m$  for nucleons with an energy of 90 MeV. The calculated values for densities ranging between  $0.08$  and  $0.2 \text{ fm}^{-3}$ , as well as those for the auxiliary mesh-points are represented by circles, triangles, x-marks, and squares for isospin asymmetries  $\beta = (\rho_n - \rho_p)/\rho$  of  $0.0, 0.2, 0.6$  and  $1$ , respectively. The corresponding polynomial interpolations are visualized in terms of a solid line for isospin symmetric nuclear matter ( $\beta = 0$ ), while the dashed line shows the interpolation for the neutron and the dotted line for the proton potentials at  $\beta > 0$ .  $U_s^m$  and  $U_0^m$  depend in a very strong but also rather smooth way on the neutron-proton asymmetry parameter  $\beta$  at all nuclear densities, as can be seen from Fig. 2.

Meanwhile, the potentials at a given density between  $0.0$  and  $0.07 \text{ fm}^{-3}$  are established with the requirement to maintain the natural tendency of microscopic DBHF curves. More details about this system will be introduced later in this section.

##### B. RMOP optimization

As mentioned above, one of the main criteria to evaluate a good optical model potential is that it can well reproduce as many of the measured scattering observables as possible. Thus, how to optimize the present microscopic potentials to predict the available experimental data sets is an important issue. Optimization procedures have widely been discussed in the literature of the optical model [21, 30]. Most of them obtain the parameters through minimizing a certain  $\chi^2$  value, given for example by

$$\chi^2 = \sum_{i=1}^P \left( \frac{\sigma_i^{\text{cal}} - \sigma_i^{\text{exp}}}{\sigma_i^{\text{exp}}} \right)^2, \quad (12)$$

where  $\sigma_i^{\text{exp}}$  is the  $i$ th experimental point,  $\sigma_i^{\text{cal}}$  is the corresponding calculated result, and  $P$  indicates the total number of experimental data in our consideration. In this study, the effective range factor  $t$  related to the Schrödinger equivalent potentials in Eq. 10, as well as the Dirac potentials at density  $\rho = 0.04$  and  $0.06 \text{ fm}^{-3}$ , remain to be determined in the optimization process. A  $\chi^2$  assessment system is specially designed to fulfill this

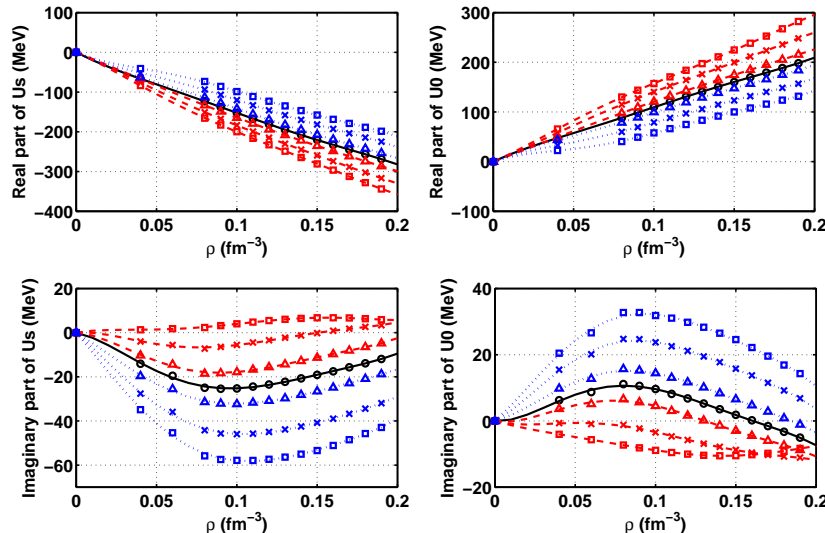


FIG. 2: (color online) Example for the real and imaginary part of the scalar ( $U_s$ ) and vector ( $U_0$ ) components of the Dirac potential as a function of density for nucleons with an incident particle energy of 90 MeV. The symbols circle, triangle, x-mark and square represent the calculated (adjusted) values for isospin asymmetries  $\beta = 0.0, 0.2, 0.6$  and  $1.0$ , respectively. The connecting solid line shows the polynomial interpolation in the case of symmetric matter, while the dashed and dotted lines visualize the corresponding interpolations for the neutron- and proton-potentials, respectively.

optimization. We employ the global simulated annealing (GSA) method based on the Monte Carlo sampling in a predefined region of the free parameters. The value of  $\chi^2/N$  is adopted as the most important criteria for this optimization procedure. Here  $\chi^2$  is defined in Eq. 12, and  $N = P - F$  is the number of degrees of freedom with the total number of experimental data  $P$  and the number of free parameters  $F$ . It is known, however, that it is not possible to obtain a 'best-fit' through the numerical optimization procedure [21] alone, therefore a visual goodness-of-fit estimation evaluator is also incorporated in our optimization procedure.

Observables including the angular distribution ( $d\sigma/d\Omega$ ), analyzing power ( $A_y$ ) for nucleon-nucleus elastic scattering as well as the neutron total cross section ( $\sigma_{tot}$ ) and proton total reaction cross section ( $\sigma_{reac}$ ) et al. have been considered in this optimization assessment system. In a first step the angular distribution of elastic scattering,  $d\sigma/d\Omega$ , is taken into account to optimize the  $\chi^2/N$  between experimental data and our theoretical calculations. After the 'minimal'  $\chi^2/N$  value is achieved for  $d\sigma/d\Omega$ , the other observables are then utilized in the visual goodness estimation for a further improvement of the MOP.

$^{40}\text{Ca}$  and  $^{208}\text{Pb}$ , for which a large number of experimental data of proton and neutron scattering were measured, are both double magic nuclei and they represent proper examples to cover a good range from isospin symmetric to asymmetric nuclei, therefore, they were selected in our MOP optimization procedure. Moreover, after optimizing the MOP using these data, we further test the potentials by predicting scattering observables of other

nuclei. As a result, our optimization procedure for proton scattering yields a value of  $t = 1.35$  fm with the value  $\chi^2/N$  of 0.29, which is a pretty good result in view of the 1028 points of  $d\sigma/d\Omega$  in 18 different experimental data sets. Similarly, we get an optimized  $t = 1.45$  fm for neutron scattering reactions. These values are comparable to the range parameter  $t = 1.4$  fm, which has been derived in our pilot study [16] focused on the target nucleus  $^{27}\text{Al}$ .

### C. Experimental database

The present MOP is assessed through a global prediction and analysis for the main observables of neutron and proton induced scattering reactions in a large mass region of  $12 \leq A \leq 209$  below incident energy 200 MeV. The most abundant natural isotopes are considered, and nuclei with even as well as odd mass numbers are incorporated.

As well known, EXFOR library is a comprehensive database to gather the nuclear reaction measurements in the world [31]. The experimental data adopted in our analysis are all referred in this library. The details of measured elastic scattering angular distribution are specified in this paper by the first author and published time, which are shown in Table I-II for neutron induced reaction and Table VI for proton incident reaction according to the diversified target nuclei. Other measurements like neutron total cross section and proton reaction cross section are also depicted in the same way in figures.

## D. Results for neutron scattering

About 500 sets of elastic scattering angular distributions, 30 sets of analyzing power angular distributions, and 20 sets of total neutron cross sections for 32 different targets are involved in this systematic comparison. The present calculations are compared with experimental data and the results from the widely-used Koning-Delaroche (KD) optical potential.

Because nucleon densities of very light nuclei are not described in a reliable way by means of the Hartree-Fock-Bogoliubov approach, we take  $^{12}\text{C}$  as the lightest target in this study. Overall, the predictions of the MOP are in rather good agreement with the experimental data as well as the results calculated by KD potential for such large mass and energy ranges. Meanwhile, it is also observed that the performance of global KD potential is satisfactory even beyond its application scope. The discussion is given in the following subsections in detail.

### 1. The neutron total cross section

The calculated neutron total cross sections of  $^{12}\text{C}$ ,  $^{56}\text{Fe}$  and  $^{208}\text{Pb}$  are compared with the experimental data and the results of KD potential in Figs. 3, 4 and 5. Within the scope of application ( $E_n > 30$  MeV), a satisfactory prediction is obtained for light nucleus  $^{12}\text{C}$ . Because more Ramsauer-like structures appear for the heavy nuclei, the data quality of prediction decrease with increasing mass number. The cross sections are underestimated in this work. The most deviation between experimental data and calculation reaches 10% for  $^{208}\text{Pb}$ .

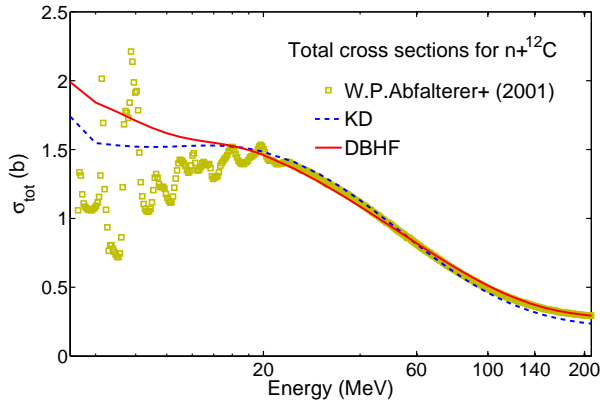


FIG. 3: (color online) Comparison of predicted neutron total cross section (solid line) and experimental data (point) and KD calculation (dashed line) for  $n + ^{12}\text{C}$ . The experimental data are measured for natural carbon.

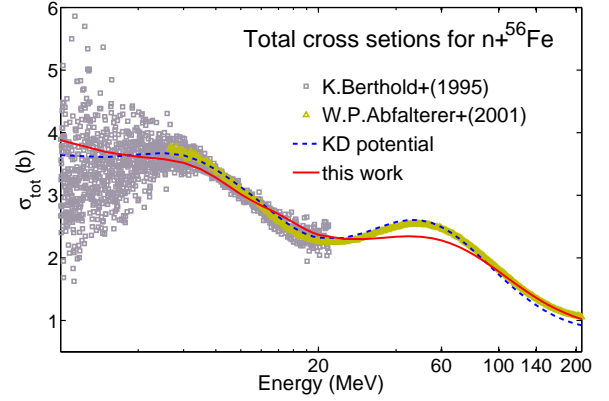


FIG. 4: (color online) Comparison of predicted neutron total cross section (solid line) and experimental data (point) and KD calculation (dashed line) for  $n + ^{56}\text{Fe}$ . The experimental data are measured for natural iron.

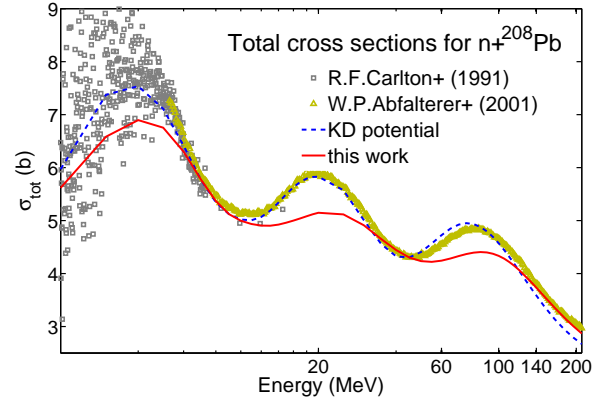


FIG. 5: (color online) Comparison of predicted neutron total cross section (solid line) and experimental data (point) and KD calculation (dashed line) for  $n + ^{208}\text{Pb}$ . The experimental data are measured for natural lead.

### 2. The elastic scattering angular distribution

As abundant experimental data are existed, we show more concern on  $d\sigma/d\Omega$  in this MOP study. Overall, the predicted results are satisfactory even below the energy scope of application of MOP. As the examples, the calculated  $d\sigma/d\Omega$  around incident neutron at 30MeV and 65MeV are plotted individually in Figs. 6 and 7, where the present predictions coincide with experimental data and the KD results very well. More details for diversified nuclei are exhibited in the following contents.

Note that for neutron elastic differential cross sections, as, e.g., in Fig. 8, the incident laboratory energies are in MeV. The curves and data points at the top are true values, while the others are offset by factors of 0.01, 0.0001, etc.

**Targets**  $^{12}\text{C}$  -  $^{40}\text{Ca}$ : 9 target nuclei including  $^{12}\text{C}$ ,  $^{14}\text{N}$ ,  $^{16}\text{O}$ ,  $^{23}\text{Na}$ ,  $^{24}\text{Mg}$ ,  $^{27}\text{Al}$ ,  $^{28}\text{Si}$ ,  $^{32}\text{S}$ , and  $^{40}\text{Ca}$  are



TABLE I: The  $d\sigma/d\Omega$  database for neutron elastic scattering

| Target   | Author(1 <sup>st</sup> ) | Year | Energy(MeV)   | Author(1 <sup>st</sup> ) | Year | Energy(MeV)   |
|----------|--------------------------|------|---|--------------------------|------|---|
| 6-C-12   | R.O.Lane                 | 1961 | 1.04, 2.25  | P.Boschung               | 1971 | 4.04  |
|          | R.M.White                | 1980 | 6.94  | G.Haouat                 | 1975 | 8.5, 9.0  |
|          | D.W.Glasgow              | 1976 | 10.69, 12.49, 13.94                                     | N.Olsson                 | 1988 | 17.6, 22.0,   |
|          | T.Niizeki                | 1990 | 35.0  | J.H.Osborne              | 2004 | 65.0, 107.5, 155, 225   |
|          | M.Ibaraki                | 2002 | 75.0  | P.Mermod                 | 2006 | 94.8  |
| 7-N-14   | J.L.Fowler               | 1955 | 1.08, 1.68, 2.07  | F.G.Perey                | 1974 | 4.34, 4.92, 6.01, 7.03, 8.56                                  |
|          | J.Chardine               | 1986 | 7.9, 9.0, 13.5  | D.Schmidt                | 2003 | 10.81, 12.79  |
|          | L.Anli                   | 1989 | 14.0, 17.0  | N.Olsson                 | 1989 | 21.6  |
| 8-O-16   | L.Drigo                  | 1976 | 2.56  | I.A.Korz                 | 1980 | 5   |
|          | G.Boerker                | 1988 | 6.37, 7.51, 9.01, 10.31, 13.61, 14.89                   | M.Baba                   | 1988 | 14.1  |
|          | L.Anli                   | 1989 | 17  | J.P.Delaroche            | 1986 | 18.0, 26.0  |
|          | N.Olsson                 | 1989 | 21.6  | P.Mermod                 | 2006 | 94.8  |
| 11-Na-23 | W.E.Kinney               | 1976 | 0.55, 0.7, 1.0, 1.2, 1.4, 1.6, 1.7, 2.0                 | U.Fasoli                 | 1969 | 1.51, 2.47, 4.04  |
|          | Th.Schweitzer            | 1978 | 3.4   | R.E.Coles                | 1971 | 5.0   |
|          | F.G.Perey                | 1970 | 5.44, 6.37, 7.6, 8.52                                   | P.Kuijper                | 1972 | 14.8  |
| 12-Mg-24 | D.B.Thomson              | 1962 | 3.79  | I.A.Korz                 | 1994 | 5.0, 6.0, 7.0   |
|          | W.E.Kinney               | 1970 | 7.55, 8.56  | M.Adel-Fawzy             | 1985 | 8.0, 9.0, 10.0, 11.0, 12.0                                    |
|          | A.Virdis                 | 1981 | 9.76, 14.8  | A.Takahashi              | 1987 | 14.1  |
|          | N.Olsson                 | 1987 | 21.6  |                          |      |   |
| 13-Al-27 | R.L.Becker               | 1966 | 3.2   | W.E.Kinney               | 1970 | 5.44, 6.44, 7.54, 8.56  |
|          | G.Dagge                  | 1989 | 7.62  | C.S.Whisnant             | 1984 | 10.87, 13.88, 16.9  |
|          | M.M.Nagadi               | 2003 | 15.4  | J.S.Petler               | 1985 | 18.20, 22.25, 26.0  |
|          | A.Bratenahl              | 1950 | 84.0  | G.L.Salmon               | 1960 | 96.0  |
|          | C.P.Van.Zyl              | 1956 | 136.0   |                          |      |   |
| 14-Si-28 | W.E.Kinney               | 1970 | 5.44, 6.37, 6.44, 7.55, 8.56                            | C.R.Howell               | 1988 | 7.96, 9.95, 11.94, 13.97, 16.92                               |
|          | J.Rapaport               | 1977 | 11.0, 20.0, 25.0  | R.Alarcon                | 1986 | 21.7  |
|          | M.Ibaraki                | 2002 | 55.0, 65.0, 75.0  |                          |      |   |
| 15-P-31  | K.Tsukada                | 1961 | 3.5,3.8,4.2,4.5   | J.Martin                 | 1968 | 5.95  |
|          | J.D.Brandenberge         | 1972 | 7.79,9.05   | P.H.Stelson              | 1965 | 14.0  |
|          | G.C.Bonazzola            | 1965 | 14.2  |                          |      |   |
| 16-S-32  | F.G.Perey                | 1970 | 3.4, 7.05, 7.6, 8.52                                    | S.Tanaka                 | 1969 | 5.92  |
|          | C.R.Howell               | 1988 | 7.96, 9.95, 11.93, 13.92                                | J.D.Brandenberge         | 1972 | 9.05  |
|          | A.Virdis                 | 1981 | 9.76  | J.Rapaport               | 1977 | 20.0, 26.0  |
|          | Y.Yamanouti              | 1977 | 21.5  | R.Alarcon                | 1986 | 21.7  |
|          | J.S.Winfield             | 1986 | 30.3, 40.3  |                          |      |   |
| 19-K-39  | J.H.Towle                | 1965 | 1.49, 2.38  | J.D.Reber                | 1967 | 2.06, 3.74, 4.33, 6.52, 7.91                                  |
|          | A.J.Frasca               | 1966 | 14.0  |                          |      |   |
| 20-Ca-40 | J.D.Reber                | 1967 | 2.06, 3.29, 5.3, 7.91                                   | B.Holmqvist              | 1969 | 6.09, 7.05  |
|          | W.Tornow                 | 1982 | 9.91, 11.9, 13.9  | G.M.Honore               | 1986 | 16.9  |
|          | R.Alarcon                | 1987 | 19.0, 25.5  | J.Rapaport               | 1977 | 20.0  |
|          | N.Olsson                 | 1987 | 21.6  | R.P.Devito               | 1981 | 30.3  |
|          | E.L.Hjort                | 1994 | 65.0  | J.H.Osborne              | 2004 | 107.5, 185.0  |
| 22-Ti-48 | A.B.Smith                | 1998 | 4.5, 5.5, 6.5, 7.55, 8.08, 8.41, 9.06, 9.5, 9.99        | C.St.Pierre              | 1959 | 14.0  |
| 24-Cr-52 | B.Holmqvist              | 1969 | 3.4   | W.E.Kinney               | 1974 | 4.34, 4.92, 6.44, 8.56  |
|          | A.B.Smith                | 1997 | 7.52  | D.Schmidt                | 1998 | 7.95, 9.0, 9.8, 10.79, 11.44, 12.01, 12.7, 13.65, 14.1, 14.76 |
|          | N.Olsson                 | 1987 | 21.6  |                          |      |   |
| 25-Mn-55 | B.Holmqvist              | 1969 | 2.47, 3.0, 3.49, 4.0, 4.56, 6.09, 7.05, 8.05            | Th.Schweitzer            | 1978 | 3.4   |
|          | A.Takahashi              | 1992 | 14.1  |                          |      |   |
| 26-Fe-56 | V.M.Morozov              | 1972 | 1.8   | W.E.Kinney               | 1968 | 4.6, 5.0, 5.56, 6.12, 6.53, 7.55                              |
|          | P.Boschung               | 1971 | 5.05  | Ruan.Xichao              | 2009 | 8.17  |
|          | S.Mellema                | 1983 | 11.0, 20, 26  | N.Olsson                 | 1987 | 21.6  |
|          | T.P.Stuart               | 1962 | 24.8  | M.Ibaraki                | 2002 | 55.0, 65.0, 75.0  |
| 27-Co-59 | B.Holmqvist              | 1969 | 1.46, 2.0, 2.47, 3.0, 3.49, 4.0, 4.56, 6.09, 7.05, 8.05 | M.M.Nagadi               | 2003 | 9.95, 15.43, 16.88, 18.86                                     |
|          | L.F.Hansen               | 1985 | 14.6  | N.Olsson                 | 1987 | 21.6  |
|          | S.T.Lam                  | 1985 | 23.0  |                          |      |   |
| 28-Ni-58 | B.Holmqvist              | 1969 | 3.0   | W.E.Kinney               | 1974 | 4.34, 6.44, 7.54, 8.56  |
|          | A.B.Smith                | 1992 | 5.5, 6.5, 8.4, 9.5, 9.99                                | P.P.Guss                 | 1985 | 7.9, 9.96, 13.94  |
|          | E.G.Christodoulo         | 1999 | 14.0  | A.Takahashi              | 1992 | 14.1  |
|          | R.S.Pedroni              | 1988 | 16.9  | N.Olsson                 | 1987 | 21.6  |
|          | Y.Yamanouti              | 1979 | 24.0  |                          |      |   |



TABLE II: The  $d\sigma/d\Omega$  database for neutron elastic scattering (continued)

| Target    | Author(1 <sup>st</sup> ) | Year | Energy(MeV)  | Author(1 <sup>st</sup> ) | Year | Energy(MeV)                        |
|-----------|--------------------------|------|--|--------------------------|------|------------------------------------|
| 29-Cu-63  | P.Guenther               | 1986 | 1.6, 2.3, 3.9  | W.E.Kinney               | 1974 | 5.5, 7.0, 8.5                      |
|           | S.M.El-Kadi              | 1982 | 7.96, 9.94, 11.93, 13.92                                       | J.D.Anderson             | 1959 | 14.6                               |
|           | B.Ya.Guzhovskiy          | 1961 | 15.0   | A.Begum                  | 1979 | 16.1                               |
|           | A.Bratenahl              | 1950 | 84.0   | G.L.Salmon               | 1960 | 96.0                               |
|           | C.P.Van.Zyl              | 1956 | 136.0  |                          |      |                                    |
| 34-Se-80  | R.M.Musaelyan            | 1987 | 0.34   | E.S.Konobeevskij         | 1984 | 1.19                               |
|           | I.A.Korzh                | 1983 | 1.5, 2.0, 2.5, 3.5   | G.V.Gorlov               | 1964 | 4                                  |
|           | R.G.Kurup                | 1984 | 8.0, 10.0  |                          |      |                                    |
| 38-Sr-88  | S.A.Cox                  | 1972 | 0.886  | M.Walt                   | 1954 | 1                                  |
|           | D.W.Kent                 | 1962 | 3.66   | V.I.Popov                | 1971 | 4.37                               |
|           | D.E.Bainum               | 1978 | 11   |                          |      |                                    |
| 39-Y-89   | R.D.Lawson               | 1986 | 4.5, 5.0, 5.5, 5.9, 6.5, 7.14, 7.5, 8.03, 8.4, 9.06, 9.5, 9.99 | F.G.Perey                | 1970 | 7.6, 8.56                          |
|           | G.M.Honore               | 1986 | 7.96, 9.95, 11.94, 13.93                                       | S.Mellema                | 1987 | 11.0                               |
|           | N.Olsson                 | 1987 | 21.6   |                          |      |                                    |
| 40-Zr-90  | P.Guenther               | 1975 | 2.0, 2.2, 2.6, 3.4   | R.W.Stooksberry          | 1976 | 2.11                               |
|           | S.Chiba                  | 1992 | 4.5, 5.0, 5.5, 5.9, 6.5, 8.03, 9.06, 9.99                      | Y.Wang                   | 1990 | 10.0, 24.0                         |
|           | D.E.Bainum               | 1978 | 11.0   | M.Ibaraki                | 2002 | 55.0, 65.0, 75.0                   |
| 41-Nb-93  | A.B.Smith                | 1985 | 4.5, 5.0, 5.5, 5.9, 6.5, 7.14, 7.5, 8.03, 8.4, 9.06            | R.S.Pedroni              | 1991 | 7.95, 9.94, 11.93, 13.92, 16.91    |
|           | J.C.Ferrer               | 1977 | 11.0   | E.G.Christodoulo         | 1999 | 14.0                               |
|           | R.Finlay                 | 1991 | 20.0   |                          |      |                                    |
| 42-Mo-98  | P.Lambropoulos           | 1973 | 1.5  | A.B.Smith                | 1975 | 2.0, 3.0, 4.0                      |
|           | J.Rapaport               | 1979 | 7.0, 9.0, 11.0, 16.0, 20.0, 26.0                               |                          |      |                                    |
| 45-Rh-103 | A.B.Smith                | 1994 | 4.51, 5.0, 5.9, 6.5, 7.5, 8.03, 8.4, 9.06, 9.5, 10.0           |                          |      |                                    |
| 49-In-115 | S.A.Cox                  | 1972 | 0.87   | B.Holmqvist              | 1969 | 3.0, 4.0, 7.05, 8.05               |
|           | A.B.Smith                | 1984 | 3.05, 3.75   | R.L.Becker               | 1966 | 3.2                                |
|           | S.Chiba                  | 1990 | 4.5, 5.0, 5.9, 7.14, 8.03, 9.06, 9.99                          | J.C.Ferrer               | 1977 | 11.0                               |
|           | J.O.Elliot               | 1956 | 14.0   | L.F.Hansen               | 1985 | 14.6                               |
| 50-Sn-120 | S.Tanaka                 | 1972 | 1.52, 2.05, 2.57, 3.08   | C.Budtz-Jorgense         | 1984 | 3.0, 3.2, 3.4, 3.6, 3.8, 4.0       |
|           | R.M.Wilenzick            | 1965 | 6.04   | P.P.Guss                 | 1989 | 9.94, 13.92, 16.91                 |
|           | J.Rapaport               | 1980 | 11.0   | T.P.Stuart               | 1962 | 24.0                               |
|           | E.L.Hjort                | 1994 | 65.0   |                          |      |                                    |
| 79-Au-197 | R.B.Day                  | 1965 | 0.5, 2.5   | F.T.Kuchnir              | 1968 | 0.6, 1.6                           |
|           | S.A.Cox                  | 1972 | 0.878, 2.0   | A.B.Smith                | 2005 | 4.51, 5.51, 6.51, 7.51, 8.41, 9.99 |
|           | S.C.Buccino              | 1966 | 5  | M.A.Etemad               | 1973 | 7                                  |
|           | B.Holmqvist              | 1971 | 8.05   | L.F.Hansen               | 1985 | 14.6                               |
| 82-Pb-208 | V.M.Morozov              | 1972 | 1.8  | J.R.M. Annand            | 1985 | 4.0, 5.0, 6.7                      |
|           | D.Schmidt                | 1996 | 7.93, 8.98, 9.87, 10.96, 11.92, 13.12, 14.23                   | W.E.Kinney               | 1974 | 8.5                                |
|           | J.Rapaport               | 1978 | 11.0, 26.0   | A.Takahashi              | 1987 | 14.1                               |
|           | R.W.Finlay               | 1984 | 20.0, 22.0, 24.0   | R.P.Devito               | 1980 | 30.3, 40.0                         |
|           | M.Ibaraki                | 2002 | 55, 65.0, 75.0   | A.Bratenahl              | 1950 | 84.0                               |
|           | J.H.Osborne              | 2004 | 85.0, 95.0, 107.0, 127.5, 155.0, 185.0, 225.0                  | A.Oehrn                  | 2008 | 96.0                               |
|           | C.P.Van.Zyl              | 1956 | 136.0  |                          |      |                                    |
|           |                          |      |  |                          |      |                                    |
| 83-Bi-209 | N.Olsson                 | 1982 | 1.48, 1.97, 2.23, 3.05   | J.R.M. Annand            | 1985 | 4.0, 5.0, 5.5, 6.5, 7.0            |
|           | R.K.Das                  | 1990 | 7.5, 8.0, 9.0, 10.0, 11.0, 12.0, 20.0, 24.0                    | N.Olsson                 | 1987 | 21.6                               |

examined in this mass region. Only  $^{40}\text{Ca}$  was considered in the optimization procedure as the example for an isospin symmetric nucleus while the results obtained for the other nuclei can be considered as predictions of

our model. The resulting  $\chi^2/N$  are tabulated in Table III. The results for all nuclei are smaller than 1.0, except for the target nucleus  $^{12}\text{C}$ . It is remarkable that the results obtained for the phenomenological KD potential

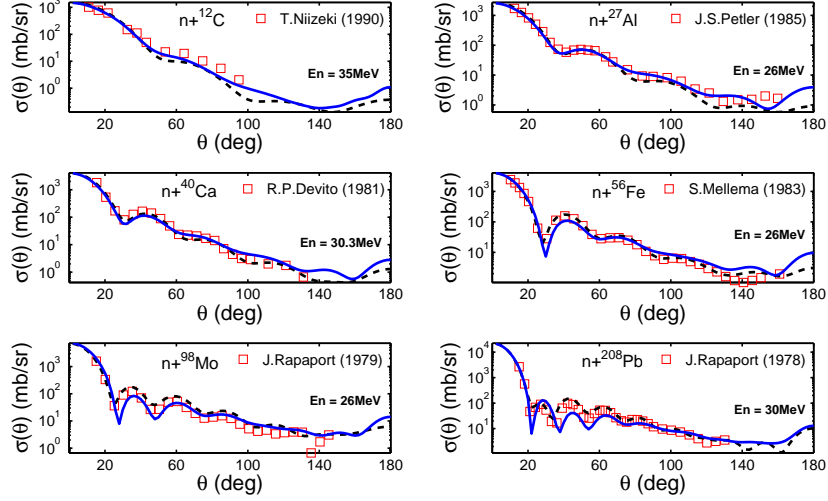


FIG. 6: (color online) Comparisons of angular distributions for  $n + {}^{12}\text{C}$ ,  ${}^{27}\text{Al}$ ,  ${}^{40}\text{Ca}$ ,  ${}^{56}\text{Fe}$ ,  ${}^{98}\text{Mo}$  and  ${}^{208}\text{Pb}$  at incident neutron energy around 30 MeV. The dashed line indicates the results from KD potential and the solid line denotes the present prediction.

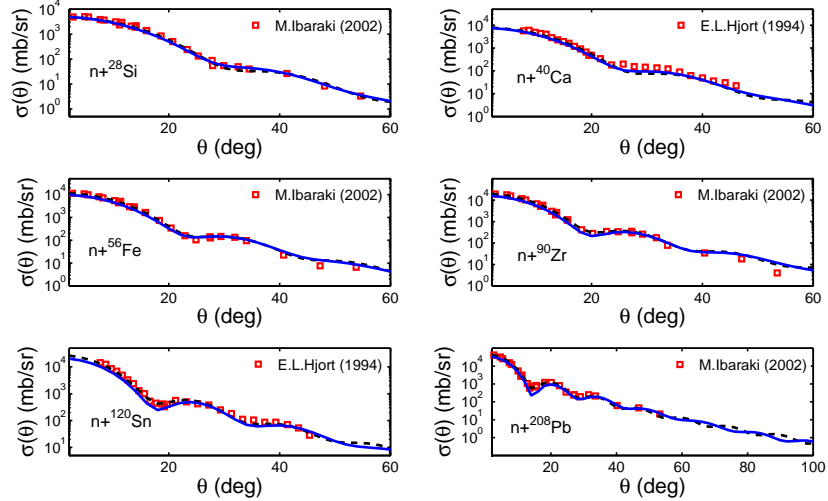


FIG. 7: (color online) Comparisons of angular distributions for  $n + {}^{28}\text{Si}$ ,  ${}^{40}\text{Ca}$ ,  ${}^{56}\text{Fe}$ ,  ${}^{90}\text{Zr}$ ,  ${}^{120}\text{Sn}$  and  ${}^{208}\text{Pb}$  at incident neutron energy around 65 MeV. The dashed line indicates the results from KD potential and the solid line denotes the present prediction.

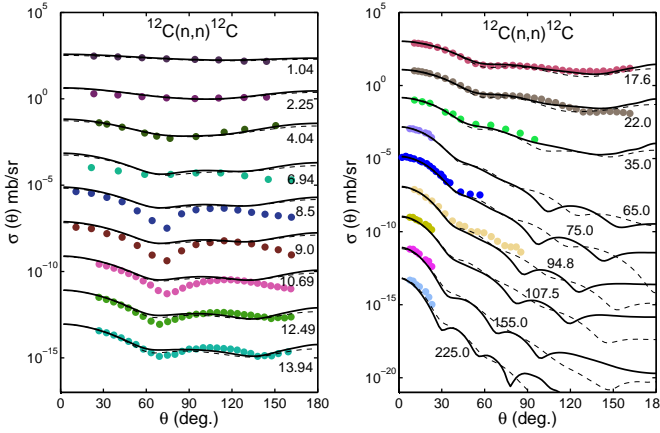
exhibit the same trends as can be observed in the microscopic optical potential. For some target nuclei like e.g.  ${}^{27}\text{Al}$  both models yield a very small value for  $\chi^2/N$  while both models yield a rather poor result for other nuclei, like e.g.  ${}^{12}\text{C}$ . The scattering on such nuclei is very much influenced by the existence of specific surface excitation modes, which cannot be described in terms of a global optical model (see discussion above). It is worth mentioning that the value for  $\chi^2/N$  for  ${}^{40}\text{Ca}$ , which has been included in the fit procedure, is comparable to the corresponding value for the other nuclei, which have not been considered in the optimization procedure.

The visual comparisons of the present predictions for  ${}^{12}\text{C}$ ,  ${}^{27}\text{Al}$  and  ${}^{40}\text{Ca}$  with the experimental data, as well as those with KD potential are shown in Figs. 8, 9 and 10. An excellent agreement with experimental data for  $n + {}^{27}\text{Al}$  is observed in Fig. 9, as already indicated in the corresponding value for  $\chi^2/N$  in Table III. From the results displayed in Fig. 8 one can see that main contributions to the large value of  $\chi^2/N$  for  ${}^{12}\text{C}$  originate from the deviations between measurements and theoretical results at the energies around  $E_n = 7$  MeV to 13 MeV. The results for  ${}^{40}\text{Ca}$  by MOP is good except for a slight underestimation at energies 10 MeV - 20 MeV around the angles

TABLE III: The  $\chi^2/N$  of  $d\sigma/d\Omega$  for  $n+^{12}\text{C} - ^{40}\text{Ca}$  reaction:

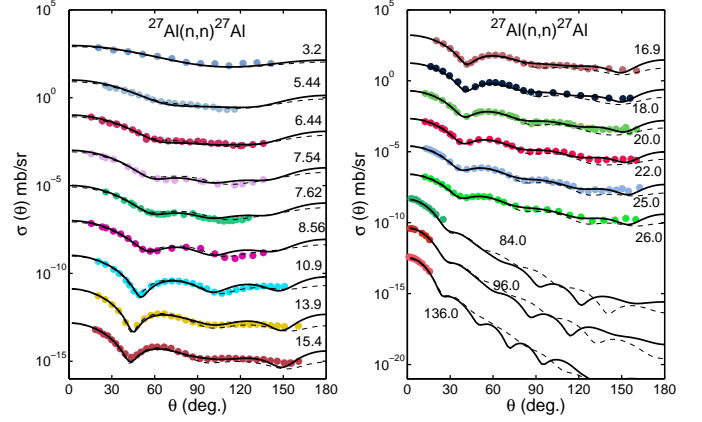
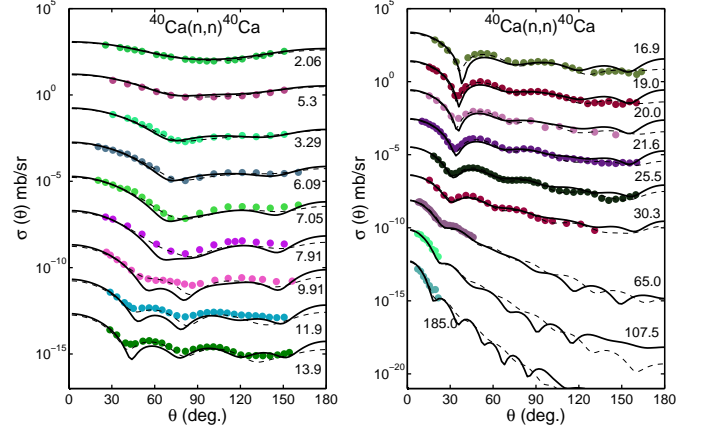
| Nuclide          | N of data points | MOP   | KD    |
|------------------|------------------|-------|-------|
| $^{12}\text{C}$  | 293              | 3.35  | 2.43  |
| $^{14}\text{N}$  | 336              | 0.21  | 0.22  |
| $^{16}\text{O}$  | 309              | 0.91  | 0.66  |
| $^{23}\text{Na}$ | 221              | 0.31  | 0.22  |
| $^{24}\text{Mg}$ | 270              | 0.56  | 0.19  |
| $^{27}\text{Al}$ | 426              | 0.068 | 0.068 |
| $^{28}\text{Si}$ | 391              | 0.24  | 0.15  |
| $^{32}\text{S}$  | 388              | 0.22  | 0.07  |
| $^{40}\text{Ca}$ | 399              | 0.22  | 0.075 |

between  $30^\circ$  to  $60^\circ$ , while the phenomenological results describe the data in this region in a very reasonable way.

FIG. 8: (color online) Comparison of predicted  $d\sigma/d\Omega$  (solid line) and experimental data (point) and KD calculation (dashed line) for  $n + ^{12}\text{C}$ .

**Targets  $^{48}\text{Ti}$ - $^{63}\text{Cu}$ :** We compare results for 5 nuclei in this mass region, which are important components of structure materials:  $^{48}\text{Ti}$ ,  $^{52}\text{Cr}$ ,  $^{56}\text{Fe}$ ,  $^{58}\text{Ni}$ , and  $^{63}\text{Cu}$ . The values of  $\chi^2/N$  are suspended around 0.11-0.17 except for a slightly larger value of 0.23 for  $^{56}\text{Fe}$  (see Table IV). As an example we show our prediction for  $^{56}\text{Fe}$  in Fig. 11 and compare it with the experimental data and the results of corresponding calculations using the phenomenological KD model. Over all our results show a fairly good agreement with the experimental data. The largest discrepancies occur for incident energies around 10 MeV to 20 MeV in a region of scattering angles between  $30^\circ$  -  $90^\circ$ . In fact, this deviation appears throughout this mass region.

**Targets  $^{80}\text{Se}$ - $^{209}\text{Bi}$ :** 13 nuclei including  $^{80}\text{Se}$ ,  $^{88}\text{Sr}$ ,  $^{89}\text{Y}$ ,  $^{90}\text{Zr}$ ,  $^{93}\text{Nb}$ ,  $^{98}\text{Mo}$ ,  $^{103}\text{Rh}$ ,  $^{115}\text{In}$ ,  $^{120}\text{Sn}$ ,  $^{140}\text{Ce}$ ,  $^{197}\text{Au}$ ,  $^{208}\text{Pb}$  and  $^{209}\text{Bi}$  are utilized to test the performance of this MOP. Good agreement is obtained generally, which could be perceived through the criteria  $\chi^2/N$  in Table V and Figs. 12 and 13 for  $^{98}\text{Mo}$ ,  $^{103}\text{Rh}$  and  $^{208}\text{Pb}$ . It is noticed that the deviation in the minimum of the an-

FIG. 9: (color online) Comparison of predicted  $d\sigma/d\Omega$  (solid line) and experimental data (point) and KD calculation (dashed line) for  $n + ^{27}\text{Al}$ .FIG. 10: (color online) Comparison of predicted  $d\sigma/d\Omega$  (solid line) and experimental data (point) and KD calculation (dashed line) for  $n + ^{40}\text{Ca}$ .

gular distribution at scattering angles  $30^\circ$  -  $60^\circ$  around  $E_n = 20$  MeV, which has been discussed above for  $^{48}\text{Ti}$ - $^{63}\text{Cu}$  also shows up for these nuclei. The results near the incident energy 20 MeV - 30 MeV generally exhibit the underestimation around  $50^\circ$ , which is illustrated also by  $d\sigma/d\Omega$  for  $^{208}\text{Pb}$  in Fig. 13. Apart from these defects above, all the  $d\sigma/d\Omega$  for other heavy target nuclei are

TABLE IV: The  $\chi^2/N$  of  $d\sigma/d\Omega$  for  $n+^{48}\text{Ti} - ^{63}\text{Cu}$  reactions

| Nuclide          | Point num. of exp. | MOP  | KD   |
|------------------|--------------------|------|------|
| $^{48}\text{Ti}$ | 378                | 0.13 | 0.05 |
| $^{52}\text{Cr}$ | 562                | 0.16 | 0.03 |
| $^{56}\text{Fe}$ | 333                | 0.23 | 0.09 |
| $^{58}\text{Ni}$ | 701                | 0.17 | 0.11 |
| $^{63}\text{Cu}$ | 282                | 0.11 | 0.06 |

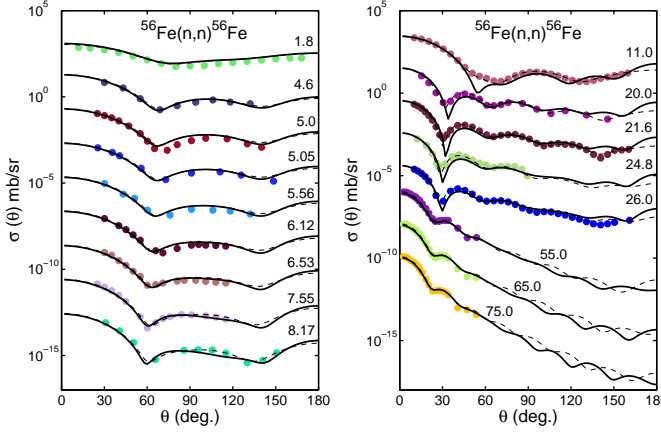


FIG. 11: (color online) Comparison of predicted  $d\sigma/d\Omega$  (solid line) and experimental data (point) and KD calculation (dashed line) for  $n + {}^{56}\text{Fe}$ .

TABLE V: The  $\chi^2/N$  of  $d\sigma/d\Omega$  for  $n + {}^{80}\text{Se}$ - ${}^{209}\text{Bi}$  reactions

| Nuclide             | Point num. of exp. | MOP  | KD   |
|---------------------|--------------------|------|------|
| ${}^{80}\text{Se}$  | 152                | 0.17 | 0.11 |
| ${}^{88}\text{Sr}$  | 81                 | 0.09 | 0.03 |
| ${}^{89}\text{Y}$   | 620                | 0.19 | 0.05 |
| ${}^{90}\text{Zr}$  | 1110               | 0.14 | 0.05 |
| ${}^{93}\text{Nb}$  | 629                | 0.13 | 0.03 |
| ${}^{98}\text{Mo}$  | 180                | 0.30 | 0.36 |
| ${}^{103}\text{Rh}$ | 400                | 0.12 | 0.06 |
| ${}^{115}\text{In}$ | 744                | 0.10 | 0.05 |
| ${}^{120}\text{Sn}$ | 357                | 0.08 | 0.03 |
| ${}^{140}\text{Ce}$ | 105                | 0.19 | 0.05 |
| ${}^{197}\text{Au}$ | 390                | 0.22 | 0.10 |
| ${}^{208}\text{Pb}$ | 885                | 2.25 | 1.86 |
| ${}^{209}\text{Bi}$ | 767                | 0.27 | 0.06 |

reproduced in a very nice way.

### 3. The analyzing power

As mentioned above, it is the important feature of the relativistic description that the spin-orbit term can be naturally involved in the scheme without any additional parameter, which is beneficial to derive the spin-orbit observables  $A_y(\theta)$  and  $Q_y(\theta)$ . The  $A_y(\theta)$  at incident energies around 10 MeV are selected to show the ability of predictions for  ${}^{12}\text{C}$ ,  ${}^{40}\text{Ca}$ ,  ${}^{58}\text{Ni}$  and  ${}^{208}\text{Pb}$  in Fig. 14, and good agreements with the experimental data for all nuclei are obtained.

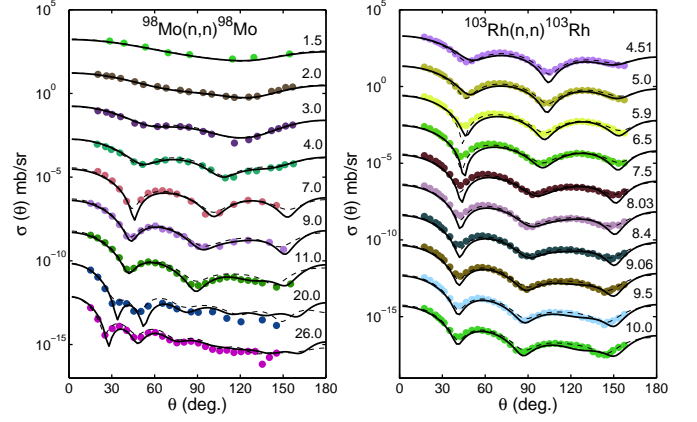


FIG. 12: (color online) Comparison of predicted  $d\sigma/d\Omega$  (solid line) and experimental data (point) and KD calculation (dashed line) for  $n + {}^{98}\text{Mo}$  and  ${}^{103}\text{Rh}$ .

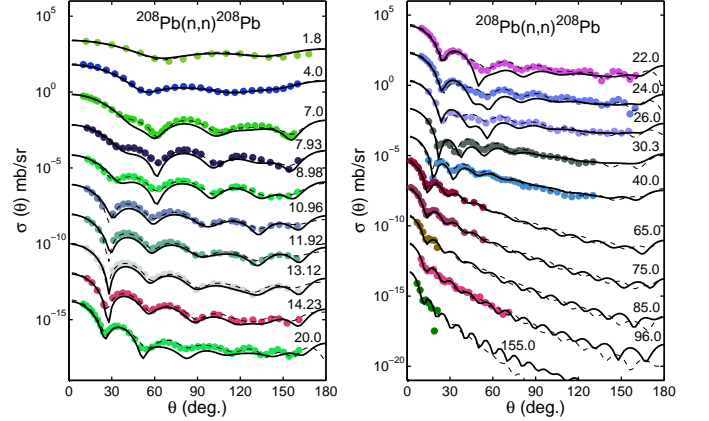


FIG. 13: (color online) Comparison of predicted  $d\sigma/d\Omega$  (solid line) and experimental data (point) and KD calculation (dashed line) for  $n + {}^{208}\text{Pb}$ .

## E. Results for proton scattering

About 150 elastic scattering angular distributions, 65 analyzing powers, and reaction cross sections of 10 commonly targets have been included in our systematic comparison. The experimental database of  $d\sigma/d\Omega$  is summarized in Table VI and depicted by the first author there. As for other quantities, the experimental data for plotting are introduced in the figures.

We compare the present calculations with the experimental data and KD results. As a whole, the various proton scattering observables are predicted satisfactorily using MOP just like its performance in neutron scattering reactions, the results are discussed in the following subsections.

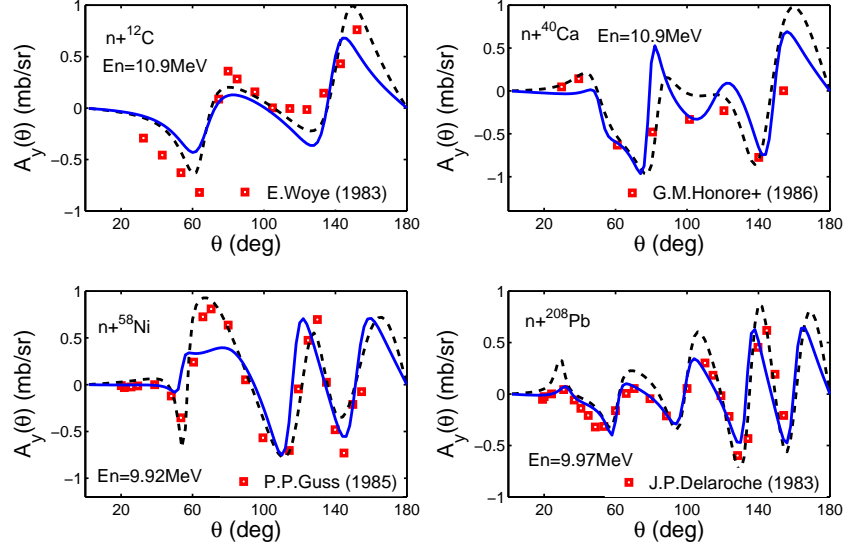


FIG. 14: (color online) Comparisons of analyzing power for  $n + {}^{12}\text{C}$ ,  ${}^{40}\text{Ca}$ ,  ${}^{58}\text{Ni}$ , and  ${}^{208}\text{Pb}$  at incident neutron energy around 10 MeV. The dashed line indicates the results from KD potential and the solid line denotes the present work.

### 1. The proton reaction cross section

It is noticed that the experimental data of proton reaction cross sections,  $\sigma_{\text{reac}}$ , are much less than  $\sigma_{\text{tot}}$  for neutron both in quantity and in quality. Therefore, we also refer to the calculated  $\sigma_{\text{reac}}$  by KD potential in the process of visual goodness-of-fit estimation. We sample the predicted  $\sigma_{\text{reac}}$  for  ${}^{40}\text{Ca}$ ,  ${}^{120}\text{Sn}$  and  ${}^{208}\text{Pb}$  in Figs. 15, 16 and 17. It can be observed that the present calculations are good but only slightly overestimate the experimental values in the whole energy region. In some cases, such as  $p + {}^{120}\text{Sn}$  in the lower energy region, this MOP looks better than the global KD. After comparisons, the maximum deviation between the predicted reaction cross sections and measurements is less than 20%.

### 2. The elastic scattering angular distribution

We collect the proton elastic scattering angular distribution just as the case for neutron. The  $d\sigma/d\Omega$  of proton scattering from 6 nuclei,  ${}^{28}\text{Si}$ ,  ${}^{40}\text{Ca}$ ,  ${}^{56}\text{Fe}$ ,  ${}^{90}\text{Zr}$ ,  ${}^{120}\text{Sn}$  and  ${}^{208}\text{Pb}$ , around proton incident energy at 65 MeV are collected in Fig. 18. The perfect agreement between the present calculations and experimental data displays the powerful prediction ability of this MOP. In addition, we also condense  $d\sigma/d\Omega$  curves of various energies belonging to the same nucleus in one figure, as in Fig. 19. Similarly, in these condensed figures, the curves and data points at the top are true values, while the others are offset by factors of 0.01, 0.0001, etc, and incident laboratory energies are in MeV.

**Targets  ${}^{12}\text{C}$ - ${}^{40}\text{Ca}$ :** with respect to the differential

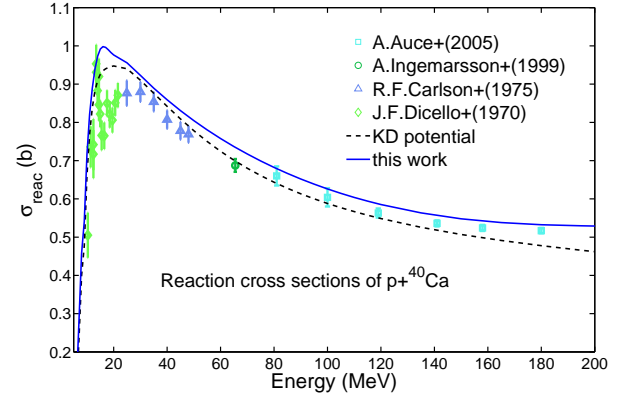


FIG. 15: (color online) Comparison of predicted reaction cross section (solid line) and experimental data (point) and KD calculation (dashed line) for  $p + {}^{40}\text{Ca}$ .

cross section  $d\sigma/d\Omega$ , the resulting  $\chi^2/N$  of nuclei in this mass region are listed in Table VII. The values for  ${}^{12}\text{C}$  and  ${}^{28}\text{Si}$  are obviously larger than for the other nuclei. To explore the source of this discrepancy, we focus our discussion on  ${}^{28}\text{Si}$  (see Fig. 19). It is observed that the theoretical results and the measurements are in good agreement within the entire angular region for incident energies  $E_p < 120$  MeV. At higher energies, however, our predictions tend to underestimate the data for the differential cross section. This feature is the main resources to cause the poor  $\chi^2/N$ .

**Targets  ${}^{48}\text{Ti}$  -  ${}^{208}\text{Pb}$ :** The  $\chi^2/N$  of  $d\sigma/d\Omega$  in this target region is shown in Table VIII. The  $\chi^2/N$  values show a good prediction in this target region. Some of them are

TABLE VI: The  $d\sigma/d\Omega$  database for proton elastic scattering

| Target    | Author(1 <sup>st</sup> ) | Year | Energy(MeV)                      | Author(1 <sup>st</sup> ) | Year | Energy(MeV)                              |
|-----------|--------------------------|------|----------------------------------|--------------------------|------|--|
| 6-C-12    | S.Mazzoni                | 1998 | 2.5                              | V.M.Lebedev              | 2006 | 7.5                                      |
|           | An-Zhu                   | 2003 | 22.0                             | M.Harada                 | 1999 | 26.0                                     |
|           | M.Ieiri                  | 1987 | 29.7, 34.5, 44.7                 | V.I.Grancev              | 1983 | 48.5                                     |
|           | A.A.Rush                 | 1971 | 50.0                             | M.Ieiri                  | 1987 | 54.4, 64.9, 74.8, 83.8                   |
|           | H.O.Meyer                | 1983 | 122.0, 160.0, 200.0, 250         | V.M.Hannen               | 2003 | 150.0                                    |
| 13-Al-27  | M.Chiori                 | 2001 | 0.783, 1.2, 3.01                 | I.E.Dayton               | 1956 | 17.0                                     |
|           | G.M.Crawley              | 1968 | 17.5                             | R.Dittman                | 1969 | 28.0                                     |
|           | C.B.Fulmer               | 1969 | 61.4                             | G.Gerstein               | 1957 | 92.9, 95.7                               |
|           | A.E.Taylor               | 1961 | 142.0                            | V.Comparat               | 1974 | 156.0                                    |
|           | A.Johansson              | 1960 | 160.0, 177.0, 183.0              | S.Dahlgren               | 1967 | 185.0                                    |
|           |                          |      |                                  |                          |      |  |
| 14-Si-28  | E.Fabrizi                | 1980 | 14.26, 17.24, 20.17, 30.5, 40.21 | M.Nakamura               | 1983 | 45.0, 50.0, 55.0, 60.0                   |
|           | S.Kato                   | 1985 | 65.0                             | C.Olmer                  | 1984 | 80.0, 100.0, 135.0, 179.0                |
|           | O.Sundberg               | 1967 | 185.0                            | K.H.Hicks                | 1988 | 200.0, 250.0                             |
| 20-Ca-40  | J.F.Dicello              | 1971 | 10.4, 14.5, 17.6, 20.6           | R.H.Mccamis              | 1986 | 25.0, 30.0, 35.0, 40.0, 45.0, 48.0       |
|           | K.Yagi                   | 1964 | 55.0                             | H.Sakaguchi              | 1982 | 65.0                                     |
|           | P.Schwandt               | 1982 | 80.0, 135.0, 160.0               | C.Rolland                | 1966 | 152.0                                    |
|           | A.Johansson              | 1961 | 182.0                            | H.Seifert                | 1993 | 201.0                                    |
|           |                          |      |                                  |                          |      |  |
| 26-Fe-56  | N.Boukharouba            | 1992 | 4.08, 5.02, 6.56, 7.74           | K.Kikuchi                | 1959 | 7.4, 14.1                                |
|           | J.Benveniste             | 1964 | 10.9                             | R.Varner                 | 1986 | 16.0                                     |
|           | I.E.Dayton               | 1956 | 17.0                             | P.Kossanyi-Demay         | 1967 | 18.6                                     |
|           | S.F.Eccles               | 1966 | 19.1                             | B.W.Ridley               | 1964 | 30.3                                     |
|           | M.K.Brussel              | 1959 | 39.8                             | F.E.Bertrand             | 1969 | 61.5                                     |
|           | H.Sakaguchi              | 1982 | 65.0                             | D.J.Steinberg            | 1964 | 146                                      |
|           | V.Comparat               | 1974 | 156.0                            | A.Johansson              | 1961 | 176                                      |
|           |                          |      |                                  |                          |      |  |
| 28-Ni-58  | L.L.Lee Jr               | 1964 | 7.0, 8.0, 9.0, 10.0, 11.0, 12.0  | S.Kobayashi              | 1960 | 14.4, 15.4                               |
|           | R.Varner                 | 1986 | 16.0                             | S.F.Eccles               | 1966 | 18.6                                     |
|           | J.R.Tesmer               | 1972 | 20.0                             | E.Fabrizi                | 1980 | 35.2                                     |
|           | L.N.Blumberg             | 1966 | 40.0                             | C.B.Fulmer               | 1969 | 61.4                                     |
|           | H.Sakaguchi              | 1982 | 65.0                             | A.Ingemarsson            | 1979 | 178.0                                    |
|           | H.Sakaguchi              | 1998 | 192.0                            | H.Takeda                 | 2003 | 250.0                                    |
|           |                          |      |                                  |                          |      |  |
| 40-Zr-90  | G.W.Greenlees            | 1971 | 9.7                              | K.Matsuda                | 1967 | 14.7                                     |
|           | R.Varner                 | 1986 | 16.0                             | J.B.Ball                 | 1964 | 22.5                                     |
|           | R.De.Swiniarski          | 1977 | 30.0                             | L.N.Blumberg             | 1966 | 40.0                                     |
|           | C.B.Fulmer               | 1969 | 61.4                             | H.Sakaguchi              | 1982 | 65.0                                     |
|           | A.Nadasen                | 1981 | 80.0, 135.0, 160.0               | V.Comparat               | 1974 | 156.0                                    |
|           | E.Hagberg                | 1971 | 185.0                            |                          |      |  |
| 50-Sn-120 | G.W.Greenlees            | 1971 | 9.7                              | R.Varner                 | 1986 | 16.0                                     |
|           | W.Makofske               | 1972 | 16.0                             | S.D.Wassenaar            | 1989 | 20.4                                     |
|           | B.W.Ridley               | 1964 | 30.3                             | L.W.Put                  | 1971 | 30.4                                     |
|           | G.S.Mani                 | 1971 | 49.4                             | F.E.Bertrand             | 1970 | 61.5                                     |
|           | S.Kailas                 | 1984 | 104.0                            | P.Schwandt               | 1982 | 135.0                                    |
|           | V.Comparat               | 1974 | 156.0                            | H.Takeda                 | 2003 | 200.0, 250.0                             |
| 82-Pb-208 | W.Makofske               | 1972 | 16.0                             | W.T.H Van Oers           | 1974 | 21.0, 24.1, 26.3, 30.3, 35.0, 45.0, 47.3 |
|           |                          |      |                                  |                          |      |  |
|           | D.W.Devins               | 1962 | 30.8                             | L.N.Blumberg             | 1966 | 40.0                                     |
|           | C.B.Fulmer               | 1969 | 61.4                             | H.Sakaguchi              | 1982 | 65.0                                     |
|           | A.Nadasen                | 1981 | 80.0, 121.0, 160.0, 182.0        | V.Comparat               | 1974 | 156.0                                    |
|           | C.Djalali                | 1982 | 201.0                            |                          |      |  |

even lower than the corresponding values by KD potential. We look through the details by considering  $d\sigma/d\Omega$  of  $^{58}\text{Ni}$  in Fig. 20. The present predictions, measurements and phenomenological KD results are consistent perfectly with each other in the entire energy region.

$^{90}\text{Zr}$  is the only example for which the  $\chi^2/N$  is not particularly good. Therefore we compare the calculated  $d\sigma/d\Omega$  for  $^{90}\text{Zr}$  in Fig.21. It is found that most theoreti-

cal values are consistent with the measurements, and the main deviations occur at specific incident energies such as 22.5 and 135.0 MeV. In addition, a very good performance of the MOP also occurs in the calculations for  $p + ^{208}\text{Pb}$ , as shown in Fig. 22.

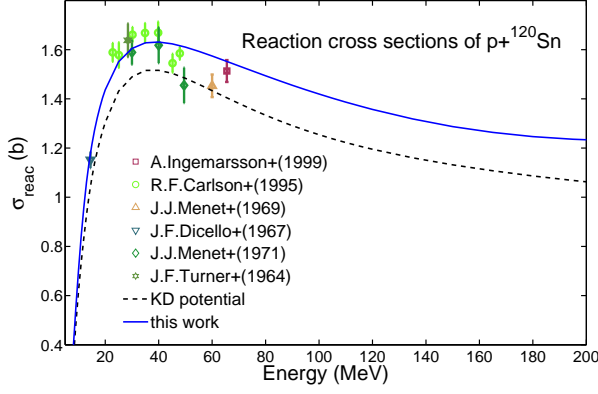


FIG. 16: (color online) Comparison of predicted reaction cross section (solid line) and experimental data (point) and KD calculation (dashed line) for  $p + {}^{120}\text{Sn}$ .

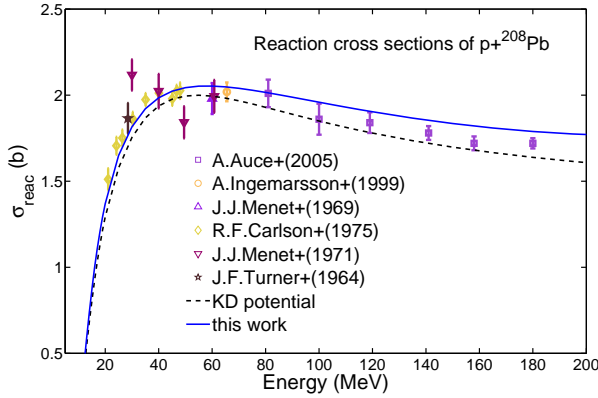


FIG. 17: (color online) Comparison of predicted reaction cross section (solid line) and experimental data (point) and KD calculation (dashed line) for  $p + {}^{208}\text{Pb}$ .

TABLE VII: The  $\chi^2/N$  of  $d\sigma/d\Omega$  for  $p + {}^{12}\text{C}$ - ${}^{40}\text{Ca}$  reactions

| Nuclide            | Point num. of exp. | MOP  | KD   |
|--------------------|--------------------|------|------|
| ${}^{12}\text{C}$  | 637                | 3.70 | 0.34 |
| ${}^{27}\text{Al}$ | 336                | 0.88 | 0.90 |
| ${}^{28}\text{Si}$ | 513                | 4.78 | 0.56 |
| ${}^{40}\text{Ca}$ | 682                | 0.37 | 0.22 |

TABLE VIII: The  $\chi^2/N$  of  $d\sigma/d\Omega$  for  $p + {}^{56}\text{Fe}$ - ${}^{208}\text{Pb}$  reactions

| Nuclide             | Point num. of exp. | MOP  | KD   |
|---------------------|--------------------|------|------|
| ${}^{56}\text{Fe}$  | 516                | 0.16 | 0.12 |
| ${}^{58}\text{Ni}$  | 557                | 0.15 | 0.13 |
| ${}^{90}\text{Zr}$  | 536                | 3.61 | 0.29 |
| ${}^{120}\text{Sn}$ | 406                | 0.27 | 0.85 |
| ${}^{208}\text{Pb}$ | 1028               | 0.29 | 0.72 |

### 3. The analyzing power and spin rotation function

The predicted analyzing power  $A_y(\theta)$  and spin rotation function  $Q(\theta)$  of proton scattering from  ${}^{208}\text{Pb}$  at  $E_p = 80$  and 200 MeV are plotted in Fig. 23. The predicted phases of  $A_y(\theta)$  and  $Q(\theta)$  look well, whereas the amplitudes are not ideal, which remain to be improved in the future. In addition, in order to show more results of other nuclei, we also plot  $A_y(\theta)$  of  ${}^{56}\text{Fe}$  and  ${}^{58}\text{Ni}$  in Fig. 24, where the applied experimental data are listed in Table IX. It is shown that the amplitudes of  $A_y(\theta)$  by MOP are better around the lower energy region.

TABLE IX: The  $A_y$  database for proton elastic scattering from  ${}^{56}\text{Fe}$  and  ${}^{58}\text{Ni}$ .

| Target   | Author(1 <sup>st</sup> ) | Year | Energy(MeV)      |
|----------|--------------------------|------|------------------|
| 26-Fe-56 | R.Varner                 | 1986 | 16.0             |
|          | P.J.Van.Hall             | 1977 | 17.2, 20.4, 24.6 |
|          | R.De.Leo                 | 1996 | 65.0             |
| 28-Ni-58 | R.Varner                 | 1986 | 16.0             |
|          | P.J.Van.Hall             | 1977 | 20.4, 24.6       |
|          | D.C.Kocher               | 1976 | 60.2             |
|          | H.Sakaguchi              | 1982 | 65.0, 192.0      |
|          | H.Takeda                 | 2003 | 250.0            |

## V. SUMMARY

The central attempt of this study is to present an optical model for nucleon-nucleus scattering, which is based on a microscopic calculation of the nucleon self-energy in nuclear matter. After adjustment of very few parameters, the new optical potential reproduces many nucleon scattering data for target nuclei across the whole nuclear mass table of stable isotopes between  ${}^{12}\text{C}$  to  ${}^{208}\text{Pb}$  at nucleon incident energies from 1 MeV to 200 MeV. The hope is that this approach for a microscopic optical potential yields reliable predictions also for unstable target nuclei, since an extrapolation in this unstable region should be more reliable than a pure phenomenological fit with more fit parameter. Of course, the specification of a sound nuclear structure for targets, especially for exotic nuclei remains to be progressed.

The microscopic basis of this study are Dirac Brueckner Hartree-Fock calculations of nuclear matter using realistic forces, which have been adjusted to describe nucleon-nucleon scattering phases. One of the basic features of this relativistic approach is that it provides a specific energy-dependence for the optical model and also predicts a spin-orbit term without the need to introduce any additional parameters (see e.g. [17]).

The complex isospin dependent self-energies are extracted from the DBHF approach with projection techniques using the Bonn-B bare  $NN$  interaction. The MOP with Bonn A has also been tested and the results show that the prediction of the scattering for finite nuclei is not



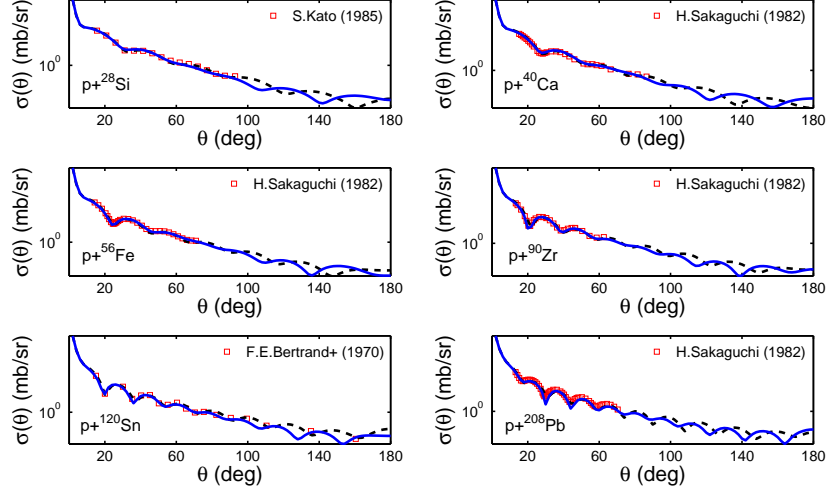


FIG. 18: (color online) Comparison of predicted angular distribution (solid line) and experimental data (point) and KD calculation (dashed line) for  $p + {}^{28}\text{Si}$ ,  ${}^{40}\text{Ca}$ ,  ${}^{56}\text{Fe}$ ,  ${}^{90}\text{Zr}$ , and  ${}^{208}\text{Pb}$  at incident neutron energy 65MeV; 61.5MeV for  $p + {}^{120}\text{Sn}$ .

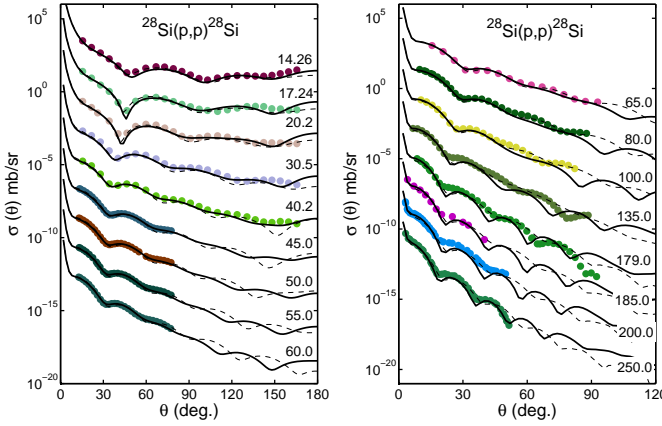


FIG. 19: (color online) Comparison of predicted  $d\sigma/d\Omega$  (solid line) and experimental data (point) and KD calculation (dashed line) for  $p + {}^{28}\text{Si}$ .

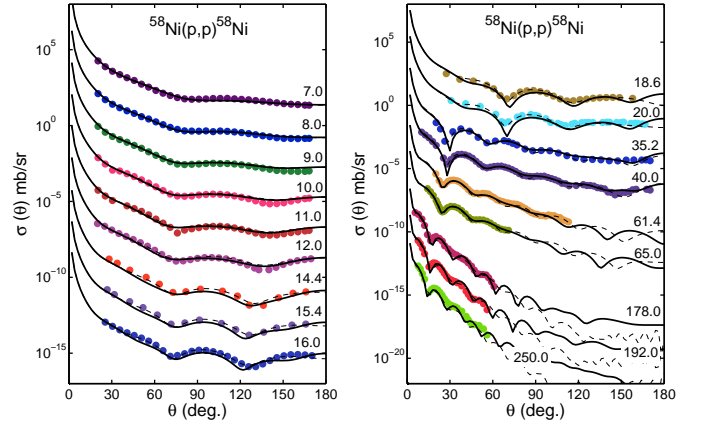


FIG. 20: (color online) Comparison of predicted  $d\sigma/d\Omega$  (solid line) and experimental data (point) and KD calculation (dashed line) for  $p + {}^{58}\text{Ni}$ .

very sensitive to the choice of a realistic nucleon force, Bonn A or Bonn B. Therefore, Bonn-B has been adopted following our pilot study [16]. The present MOP is very strictly built on the DBHF calculations in nuclear matter at  $\rho > 0.08 \text{ fm}^{-3}$  by means of the improved local density approximation. For the purpose of describing the observables of scattering, we construct the optimization method according to the annealing algorithm. The range factors in ILDA and the scalar and vector potentials below  $0.08 \text{ fm}^{-3}$  are extracted using this method from the experimental data of  ${}^{40}\text{Ca}$  as an example for isospin symmetric nuclei and  ${}^{208}\text{Pb}$  for isospin asymmetric nuclei. Then they are applied for many nuclei and energy regions. Good predictions for most nuclei are achieved by

the resulting MOP only with the free parameter  $t$ . The results of the MOP are of a quality, which is comparable to the widely used phenomenological Koning-Delaroche (KD) global potential. A bit of imperfection still exists in both  $n+A$  and  $p+A$  systems for specific target nuclei.

Certainly, it is impossible to depict all quantities in a perfect way within the spherical nuclear OM and the present MOP, especially for the strongly deformed nuclei around rare earth and actinide. Also it should be kept in mind that the MOP is based on a microscopic study of nuclear matter. Therefore all features, which are related to surface excitation, e.g. the particle-vibration coupling, are not explicitly taken into account. Such features shall be included in future studies. Moreover we plan to make

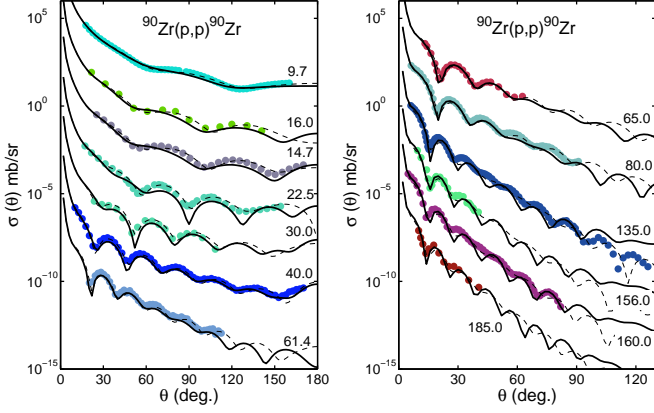


FIG. 21: (color online) Comparison of predicted  $d\sigma/d\Omega$  (solid line) and experimental data (point) and KD calculation (dashed line) for  $p + {}^{90}\text{Zr}$ .

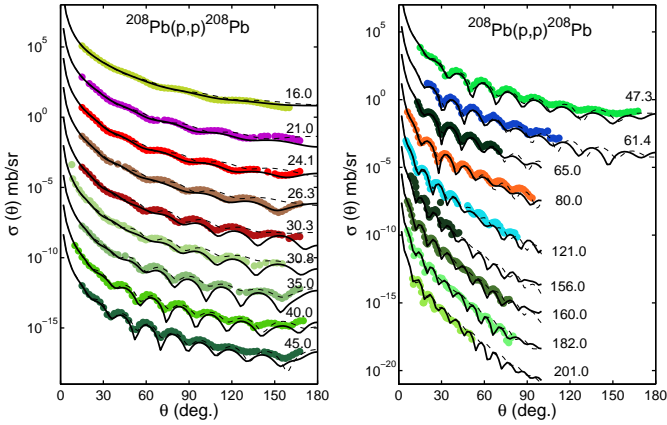


FIG. 22: (color online) Comparison of predicted  $d\sigma/d\Omega$  (solid line) and experimental data (point) and KD calculation (dashed line) for  $p + {}^{208}\text{Pb}$ .

the present MOP available in form of an interactive web-based application.

### Acknowledgments

We thank Prof. S. Hilaire for kindly supplying us all the density distributions of finite nuclei calculated in the Hartree-Fock-Bogoliubov (HFB) approach with Gogny D1S force. R. R. Xu thanks Prof. Q. B. Shen and Y. L. Han for helpful discussion on the code APMN and physics. This work has been supported by the National Basic Research Program of China under Grant No 2013CB834404 and the National Natural Science Foundation of China (Grant Nos. 11305270, 11275018); the Deutsche Forschungsgemeinschaft (DFG) under contract no. Mu 705/10-1.

- 
- [1] M. T. Pigni, M. Herman, P. Obložinský, and F. S. Dietrich, Phys. Rev. **C 83**, 024601 (2011).
  - [2] G. Blanchon, M. Dupuis, H. F. Arellano, and N. Vinh Mau, Phys. Rev. **C 91**, 014612 (2015).
  - [3] L. G. Cao, G. Colo, H. Sagawa, and P. F. Bortignon, Phys. Rev. **C 89**, 044314 (2014).
  - [4] L. Ray, G. W. Hoffmann, and W. R. Coker, Phys. Rep. **212**, 223 (1992).
  - [5] Y. L. Xu, H. R. Guo, Y. L. Han and Q. B. Shen, J. Phys. **G41**, 015101 (2014).
  - [6] J. P. Jeukenne, A. Lejeune, and C. Mahaux, Phys. Rev. **C 16**, 80 (1977).
  - [7] K. Amos, P.J. Dortmans, H.V. von Geramb, S. Karataglidis, J. Raynal, Adv. Nucl. Phys. **25**, 1 (2000).
  - [8] P. K. Deb, K. Amos, S. Karataglidis, M. B. Chadwick, and D. G. Madland, Phys. Rev. Lett. **86**, 3248 (2001).
  - [9] B. A. Brown, Phys. Rev. Lett. **85**, 5296 (2000).
  - [10] P. K. Deb, B. C. Clark, S. Hama, K. Amos, S. Karataglidis, and E. D. Cooper, Phys. Rev. **C 72**, 014608 (2005).
  - [11] A. Lagoyannis, et al., Phys. Lett. B **518**, 27 (2001).
  - [12] M. Dupuis, S. Karataglidis, E. Bauge, J. P. Delaroche, and D. Gogny, Phys. Rev. **C 73**, 014605 (2006).
  - [13] M. Dupuis, S. Karataglidis, E. Bauge and J.P. Delaroche, Phys. Lett. B **665**, 152 (2008).
  - [14] B. D. Serot and J. D. Walecka, Adv. Nucl. Phys. **16**, 1 (1986).
  - [15] E. D. Cooper, S. Hama, B. C. Clark, and R. L. Mercer, Phys. Rev. **C 47**, 297 (1993).
  - [16] R. R. Xu, Z. Y. Ma, E. N. E. van Dalen and H. Muther, Phys. Rev. **C 85**, 034613 (2012).
  - [17] E. N. E. van Dalen and H. Muther, Int. Journ of Mod. Phys. **E 19**, 2077 (2010).
  - [18] A.H. Lippok and H. Muther, Phys. Rev. **C 92**, 034312

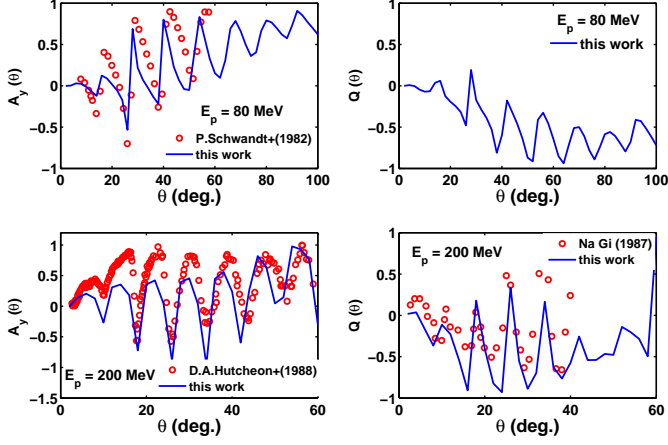


FIG. 23: (color online) Comparison of predicted  $A_y$  and  $Q$  (solid line) and experimental data (point) and KD calculation (dashed line) for  $p+^{208}\text{Pb}$  at  $E_p = 80\text{MeV}$  and  $200\text{MeV}$ . The experimental data of  $A_y$  are taken from EXFOR library, while the data of  $Q$  are read from [32].

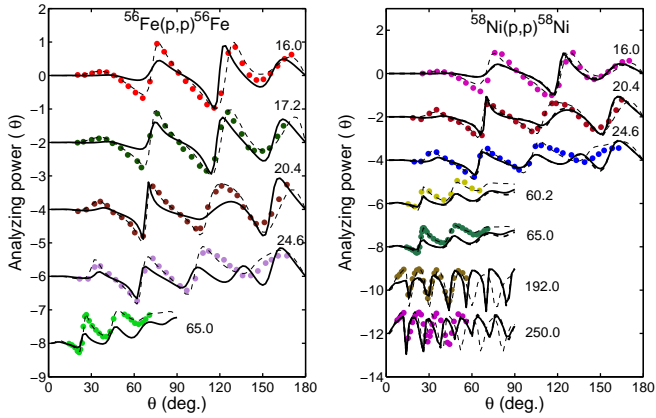


FIG. 24: (color online) Comparison of predicted  $A_y$  (solid line) and experimental data (point) and KD calculation (dashed line) for  $p+^{56}\text{Fe}$  and  $^{58}\text{Ni}$ . The curves and data points at the top represent true values, the others are offset by factors of 2, 4, 8, etc.

- (2015).
- [19] Z. H. Li, U. Lombardo, H. J. Schulze, and W. Zuo, Phys. Rev. **C 77**, 034316 (2008).
  - [20] E. N. E. van Dalen, C. Fuchs, A. Faessler, Nucl. Phys. **A744**, 227 (2004).
  - [21] A. J. Koning, J. P. Delaroche, Nucl. Phys. **A 713**, 231 (2003).
  - [22] T. Gross-Boelting, C. Fuchs, Amand Faessler, Nucl. Phys. **A648**, 105 (1999).
  - [23] Z. Y. Ma, P. Zhu, Y. Q. Gu, and Y. Z. Zhou, Nucl. Phys. **A 490**, 619 (1988).
  - [24] E. N. E. van Dalen, C. Fuchs, A. Faessler, Eur. Phys. J. **A 31**, 29 (2007).
  - [25] E. N. E. van Dalen, H. M  ther, Phys. Rev. **C 82**, 014319 (2010).
  - [26] R. Machleidt, Adv. Nucl. Phys. **19**, 189 (1989).
  - [27] S. Hilaire and M. Girod, Eur. Phys. J. **A 33**, 233 (2007).
  - [28] J. W. Negele, Phys. Rev. **C 1**, 1260 (1970).
  - [29] Q. B. Shen, Nucl. Sci. Eng. **141**, 78 (2002).
  - [30] F. G. Perey, Phys. Rev. **C 131**, 745 (1963).
  - [31] <https://www-nds.iaea.org/exfor/exfor.htm>; and V. McLane, BNL-NCS-63380-2000/05-Rev (2000).
  - [32] Ch. Elster and S. P. Weppner, Phys. Rev. **C 57**, 189 (1998) and the reference therein.